Transcriptional Changes and Oxidative Stress Associated with the Synergistic Interaction Between *Potato virus X* and *Potato virus Y* and Their Relationship with Symptom Expression

Alberto García-Marcos, Remedios Pacheco, Justo Martiáñez, Pablo González-Jara, José Ramón Díaz-Ruíz, and Francisco Tenllado

Many virus diseases of economic importance to agriculture result from mixtures of different pathogens invading the host at a given time. This contrasts with the relatively scarce studies available on the molecular events associated with virus–host interactions in mixed infections. Compared with single infections, co-infection of *Nicotiana benthamiana* with *Potato virus X* (PVX) and *Potato virus Y* (PVY) resulted in increased systemic symptoms (synergism) that led to necrosis of the newly emerging leaves and death of the plant. A comparative transcriptional analysis was undertaken to identify quantitative and qualitative differences in gene expression during this synergistic infection and correlate these changes with the severe symptoms it caused. Global transcription profiles of doubly infected leaves were compared with those from singly infected leaves using gene ontology enrichment analysis and metabolic pathway annotator software. Functional gene categories altered by the double infection comprise suites of genes regulated coordinately, which are associated with chloroplast functions (downregulated), protein synthesis and degradation (upregulated), carbohydrate metabolism (upregulated), and response to biotic stimulus and stress (upregulated). The expressions of reactive oxygen species–generating enzymes as well as several mitogen-activated protein kinases were also significantly induced. Accordingly, synergistic infection induced a severe oxidative stress in *N. benthamiana* leaves, as judged by increases in lipid peroxidation and by the generation of superoxide radicals in chloroplasts, which correlated with the misregulation of antioxidative genes in microarray data. Interestingly, expression of genes encoding oxylipin biosynthesis was uniquely upregulated by the synergistic infection. Virus-induced gene silencing of α-dioxygenase1 delayed cell death during PVX–PVY infection.

In susceptible hosts, plant viruses typically induce a number of morphological and physiological modifications in combination with an altered expression pattern of host genes. These alterations may have several consequences that include the diversion of metabolic pathways for the production of viral components, changes that either enhance virus multiplication or delay host defense responses, and the misregulation of genes involved in plant growth and development. Some of these alterations do not necessarily provide an advantage to the virus but, nevertheless, may have adverse effects on the host (Culver and Padmanabhan 2007). Unfortunately, our knowledge of the cellular processes responsible for disease response to viral infection is limited. A few reports provide insight into some of the molecular mechanisms that contribute to symptom development, such as interference with multiple metabolic signaling or host developmental pathways that include phytohormones (e.g., auxin and gibberellin) (Kong et al. 2000; Zhu et al. 2005; Padmanabhan et al. 2006), and microRNAs (Kasschau et al. 2003).

Numerous simultaneous infections with distinct plant viruses have been observed in natural situations, with biological and epidemiological implications. In many cases, a mixed infection elicits disease symptoms that are more severe than those induced in single infections by either of the viruses, a phenomenon known as synergism in pathology (Hull 2002). Virus–virus interaction in mixed infections has been suggested to result from suppression of the host defense mechanism based on RNA silencing by one or both of the interacting viruses (Vanitharani et al. 2004). Other reports suggested important roles of viral-silencing suppressor proteins in defining tissue invasion patterns in mixed-virus infections (Wege and Siegmud 2007). However, the molecular mechanisms involved in symptom development remain unresolved. For instance, little is known about transcriptomic changes associated with synergistic infections which might provide a means to link specific cellular processes to the development of the synergistic disease symptoms.

Microarray technology has emerged as a powerful tool to evaluate changes in the expression of genes as a consequence of virus infection on a genome-wide scale (Whitham et al. 2003, 2006). However, hybridization of whole-genome arrays, particularly those involving virus infections, typically produces a vast amount of expression data. Thus, although it is presumed that genes involved in symptom expression are represented within microarray data, identifying which cellular path-

ways and how they relate to symptom development remains a challenging task. In this scenario, bioinformatic tools are emerging that use ontologies to interpret expression data in terms of known biological background and, therefore, enable comprehensive interpretation at the functional level (Thimm et al. 2004; Maere et al. 2005).

Most of the reported synergistic viral diseases involve a *Potyvirus* sp. as one of the synergistic pair. The best-studied synergistic pair is the interaction between *Potato virus Y* (PVY) and *Potato virus X* (PVX) (PVX–PVY) in tobacco plants (*Nicotiana tabacum*), in which the level of PVX was enhanced 3- to 10-fold compared with singly infected plants (Vance 1991; González-Jara et al. 2004). In PVY–PVX–tobacco synergism, the RNA silencing suppressor HC-Pro of PVY allowed PVX to accumulate beyond the normal silencing-imposed limits (Pruss et al. 1997). However, the increase of disease symptoms may not be entirely due to the enhancement of PVX accumulation. The accumulation of PVX did not vary greatly in *N. benthamiana* when doubly infected with PVX and either PVY, *Tobacco etch virus*, or *Plum pox virus*, despite the extreme enhancement of symptoms in this host that lead to necrosis of leaves and stems and a rapid death of plants (González-Jara et al. 2004, 2005). This indicates that PVX titer enhancement in PVX–*Potyvirus* spp. synergistic interactions is host-dependent.

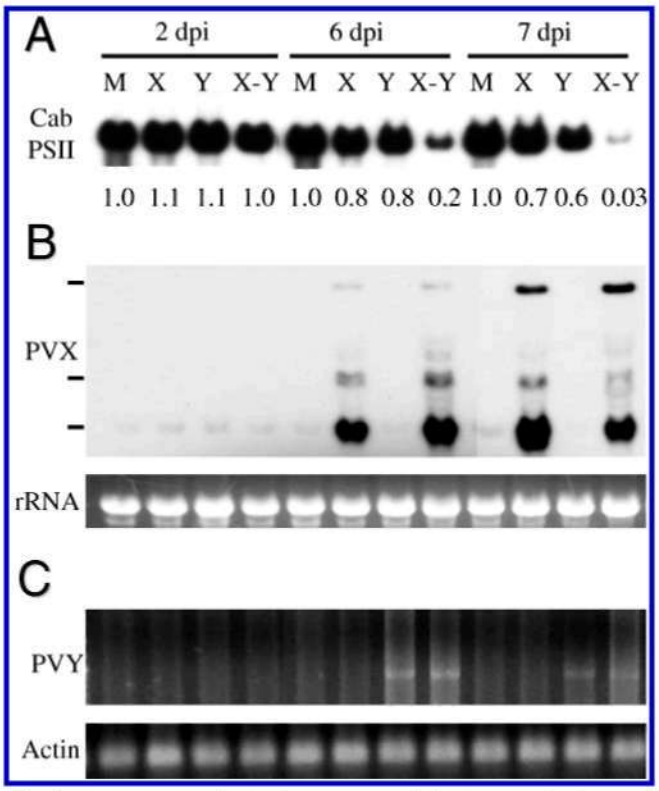

Fig. 1. Time course analysis of RNA accumulation in systemic leaves of *Nicotiana benthamiana* plants inoculated with *Potato virus X* (PVX) (X), *Potato virus Y* (PVY) (Y), PVX and PVY (X–Y), or mock inoculated (M). **A,** Northern blot hybridization showing chlorophyll a/b-binding protein (*CAB*) messenger (m)RNA accumulation using a cDNA fragment from the *CAB-E* gene as a probe. The mRNA levels were quantitated by Quantity One scanning and normalized adjusting mock-inoculated levels arbitrarily to 1.0. **B,** Northern blot hybridization showing PVX RNA accumulation using PVX coat protein (CP) sequences as a probe. Expected sizes of genomic and subgenomic PVX RNAs are indicated on the left. Ethidium bromide-stained RNA is shown as loading control. **C,** Reverse-transcriptase (RT) polymerase chain reaction amplification of a cDNA fragment corresponding to the PVY CP gene. The same RT reactions were used to amplify *Actin* gene transcripts as a control.

N. benthamiana has become an attractive host for functional genomic studies (Goodin et al. 2008). The Institute for Genomic Research (TIGR) potato cDNA array has been successfully used to investigate transcriptional changes in *N. benthamiana* in response to a number of plant viruses (Senthil et al. 2005; Dardick 2007). Moreover, virus-induced gene silencing (VIGS) can be readily applied in this host to rapidly knock down the expression of virtually any gene of interest, thus enabling the functional characterization of candidate plant genes involved in symptom development (Liu et al. 2002).

To identify gene expression changes that take place prior to the development of severe symptoms elicited by viral synergism, we performed comparative expression profiling experiments on *N. benthamiana* leaves infected with PVX, PVY, or the PVX–PVY pair. Gene ontology (GO) enrichment analysis showed several overrepresented categories in both induced and repressed gene sets derived from the double infection, which potentially were involved in viral pathogenesis and symptom expression. Furthermore, by using visualization software and reverse genetics based on VIGS, it was possible to uncover genes encoding oxylipin biosynthesis as determinants of symptom expression during PVX–PVY synergism.

RESULTS

Time-course analysis of PVX–PVY synergistic interaction.

N. benthamiana plants co-infected with PVX and PVY developed initial symptoms of vein clearing in systemically infected leaves at 6 days postinoculation (dpi) (Supplementary Fig. S1), followed by chlorotic mosaic, leaf curling, stunting, and necrosis in stems and leaves that eventually led to plant death by 12 dpi. In contrast, PVX caused the appearance of mild chlorotic mottling in systemically infected leaves whereas PVY induced leaf curling and stunting (González-Jara et al. 2004). To identify genes that regulate early events in the PVX–PVY synergistic interaction, we sought a time point for tissue collection that documents changes in host gene expression but also precludes the wide late genetic responses related to necrosis. *N. benthamiana* plants were mock inoculated, singly inoculated with PVX or PVY, or doubly inoculated with PVX and PVY, and samples were collected from upper, non-inoculated leaves at 2, 5, 6, and 7 dpi (Fig. 1 and data not shown). Preliminary observations seemed to indicate that the synergistic phenotype was associated with a decreased accumulation of messenger (m)RNAs that are related to chloroplast function. A moderate reduction (fivefold) in chlorophyll a/b-binding protein (*CAB*) mRNA levels was detected in doubly infected plants at 6 dpi (Fig. 1A). At 7 dpi, *CAB* mRNAs could hardly be detected (30-fold less than in control), suggesting severe changes in the gene expression profile of doubly infected plants. In contrast, accumulation of *CAB* mRNAs at the different time points was only slightly lower in PVX- or PVY-infected plants than in equivalent leaves from mock-inoculated plants. Similar results were found for high chlorophyll fluorescence 136 (*HCF136*) mRNA, a PSII assembly factor (data not shown).

PVX RNA was first detected at 5 dpi (data not shown) and continued to accumulate until 7 dpi (Fig. 1B). Reverse-transcriptase polymerase chain reaction (RT-PCR) analysis showed increased levels of PVY RNA at 6 dpi relative to 7 dpi (Fig. 1C). The levels of PVX RNA and PVY RNA accumulation were roughly similar in singly and doubly infected plants, in spite of the drastic differences that would manifest in symptoms afterward. Therefore, a time point for comparative gene expression profiling experiments was chosen at 6 dpi, based on significant accumulation of viral RNAs in systemic leaves,

moderate changes in the levels of chloroplast-associated mRNAs, and the earliest time that infection was manifested by the appearance of symptoms.

Microarray analysis of gene expression in *N. benthamiana* infected by diverse viruses.

A design for array hybridizations was used in which labeled aRNA derived from each virus-infected sample was hybridized with labeled aRNA from the corresponding mock-inoculated controls. This design allowed for direct comparisons between the expression profiles resulting from all three virus treatments. To assess the reliability of the microarray data, the normalized median signal intensities resulting from control samples (mock-inoculated plants) were compared across all the replicates for each treatment. A high correlation (0.94 to 0.96) among the mock-inoculated control samples was observed, indicating low technical and biological variability between the replicates.

Following statistical analysis of the data, 2,390, 1,697, and 471 expressed sequence tags (EST) were significantly altered (corrected P values $[Q] < 0.05$) in response to PVX–PVY, PVX, and PVY, respectively, with more than 1.5-fold increase or 1.5-fold decrease in signal intensity (Supplementary Table S1). Similar numbers of EST were either induced or repressed after infection by either PVX–PVY (1,239 and 1,151) or PVX (826 and 871) whereas, for PVY, more EST were induced (307) than repressed (164).

Venn analysis of selected EST showed that virus infections caused both common and specific changes in host gene expression (Fig. 2A). In all, 88.9 and 87.5% of EST altered by PVX and PVY infection, respectively, also were altered in PVX–PVY-infected plants; and, in most cases, the observed changes were in the same direction. Most EST altered by PVY infection (378 of 471, 80.2%) corresponded to the subset of EST differentially expressed in common by all three virus infections. Most striking was the finding that PVX–PVY infection uniquely altered the expression of 847 EST in the array, which represents 35.4% of EST differentially expressed by this virus treatment. In contrast, expression of a relatively small number of transcripts was uniquely changed as a consequence of either PVX (181, 10.6%) or PVY (52, 11%) infection. This suggests that PVX–PVY infection elicits a greater number of specific changes in *N. benthamiana* gene expression than single infections.

Hierarchical clustering was used to group the entire data sets from the three virus treatments by the similarity of their overall gene expression profiles. PVX and PVX–PVY samples were grouped together, indicating a closer relationship in the changes of relative transcript abundance between these infections compared with those induced by PVY. For brevity, EST with changes in expression of fourfold or more (up or down) in PVX–PVY-infected leaves were selected and then represented in Figure 2B.

Functional categorization of EST expressed differentially in response to virus infections.

We applied a Java-based tool, the Biological Networks GO tool (BiNGO), to determine which GO categories were statistically over- and underrepresented (hypergeometric test, $P < 0.05$) in each set of differentially expressed EST that were up- or downregulated by the different virus infections. No GO category was exclusively underrepresented in the induced or repressed data set from PVX–PVY. We focused on biological processes that were overrepresented in PVX–PVY infection to highlight quantitative and qualitative differences when compared with data sets from PVX or PVY. Comparative results for an intermediate level of ontology are shown in Table 1 and the complete analysis is available in Supplementary Table S2.

In all three virus infections, repressed genes predicted to encode proteins that are related to chloroplast function (photosynthesis) or localization (plastid and thylakoid) were in the most highly overrepresented categories. They included genes

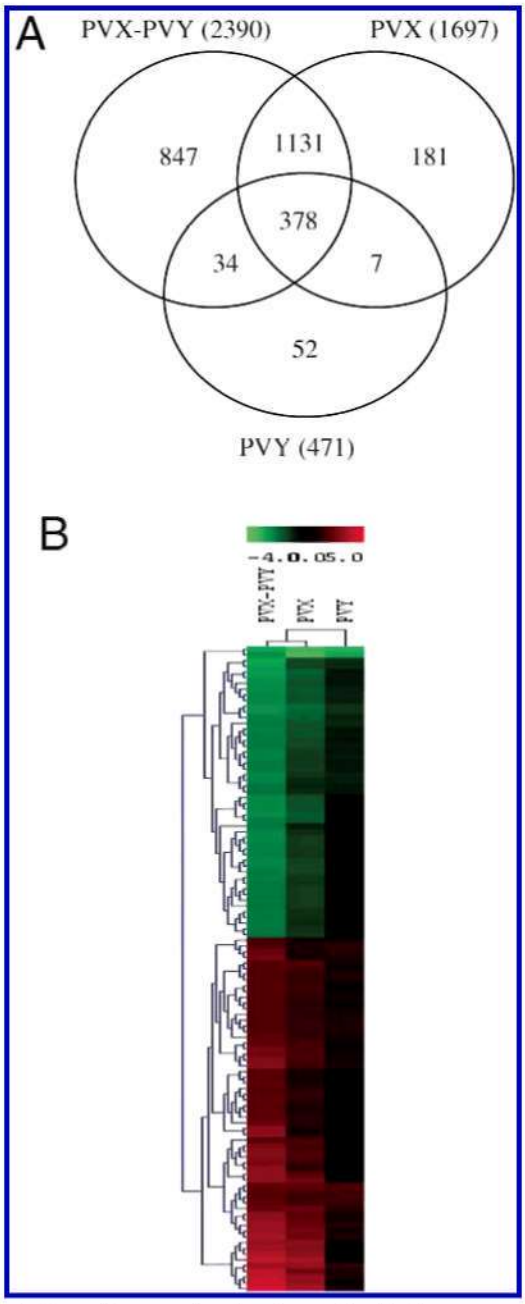

Fig. 2. A, Venn diagrams showing the relationship between expressed sequence tags (EST) that showed statistically significant (corrected P values $[Q] < 0.05$) differential expression in response to infection by *Potato virus X* (PVX), *Potato virus Y* (PVY), or PVX and PVY (PVX–PVY). Total number of EST altered by the different virus infections is given in parentheses. Numbers of EST shown in the nonoverlapping sectors represent unique significant transcripts, whereas numbers of EST shown within the intersection represent shared significant transcripts. Only genes with changes in expression of 1.5-fold or more (up or down) relative to the control are shown. **B,** Hierarchical cluster analysis of differential expression profiles for 113 EST of plants infected with PVX, PVY, or PVX–PVY. Only EST with changes in expression of fourfold or more (up or down) in PVX–PVY-infected tissue relative to the control are shown. Expression values are color-coded, with red indicating upregulation, green indicating downregulation, and black indicating no change in the expression. A $\log_2$ scale showing increase or decrease is shown at the top.

involved in light harvesting, photosynthesis, Calvin cycle, amino acid biosynthesis, and fatty acid biosynthesis. The overrepresentation of these GO categories in data sets from PVX–PVY was greater than in those from PVX or PVY, indicating a deeper impact of the synergistic infection on chloroplastic metabolism. Furthermore, the fold change of repressed genes in the photosynthesis category was greater in PVX–PVY infection than in PVX or PVY infection (Supplementary Table S3). The lipid metabolism category was the only exclusively overrepresented category in the repressed data set from PVX–PVY. Members in this category include genes involved in fatty acid biosynthesis and predicted to reside in the chloroplast, which is consistent with the findings shown above.

Several GO terms in the biological process classification were overrepresented in the induced data sets derived from all three virus treatments (protein metabolism and carbohydrate metabolism categories) or in those derived from PVX–PVY and PVY (generation of precursor metabolites and energy). Genes in the protein metabolism category encode proteins assigned to functions such as protein synthesis, chaperones, and protein degradation. Carbohydrate metabolism and generation of precursor metabolites and energy categories include genes encoding for enzymes in the trichloroacetic acid cycle, glycolysis, trehalose metabolism, and sucrose synthase, among others. Again, the virus treatment that conferred the lowest *P* values in all these categories was PVX–PVY.

There were four GO categories (protein biosynthesis, cell organization and biogenesis, response to stress, and response to biotic stimulus) exclusively overrepresented in the induced data set from PVX–PVY. Protein biosynthesis and cell organization and biogenesis categories include genes associated with translation initiation and regulation, protein glycosylation, ribosome proteins, and transport proteins (Supplementary Table S4). Accordingly, molecular function (structural molecule activity and translation regulator activity) and cellular component (ribosome) categories related to protein synthesis were also overrepresented in PVX–PVY treatment (Table 1).

An apparent inconsistency was the finding that ribosome and structural molecule activity categories were overrepresented in both induced and repressed data sets derived from PVX–PVY infection. However, EST within these two categories in the repressed data set related mostly to proteins in the 30S and 50S ribosomal subunits of chloroplasts whereas those from the induced data set corresponded to cytosolic ribosomal subunits (Supplementary Table S5). This prompted us to analyze the expression data of plastid-encoded genes. Based on similarity to *Arabidopsis* counterparts, it was estimated that 26 (30%) of all plastid-encoded genes from potato were represented on the array (Dardick 2007). Despite the broad repression of chloroplast-related genes caused by PVX–PVY infection, few plastid-encoded genes were altered significantly. Of these six genes, only one was repressed by this virus treat-

Table 1. Comparative gene ontology analyses of expressed sequence tags (EST) altered by different virus treatments[a]

Description	No. of total EST	Virus	No. of expressed EST	*P*
Repressed data sets				
Biological process				
Photosynthesis	41	**PVX-PVY**	39	1.76E-33
		PVX	32	1.66E-25
		PVY	8	2.36E-06
Generation of precursor metabolites and energy	186	**PVX-PVY**	43	2.05E-05
		PVX	38	2.36E-06
		PVY	10	3.01E-03
Lipid metabolism	186	**PVX-PVY**	34	1.42E-02
		PVX	20	5.56E-01
		PVY	3	1.00E+00
Molecular function				
Electron transport	117	**PVX-PVY**	28	4.74E-04
		PVX	27	9.74E-06
		PVY	8	2.40E-03
Structural molecule activity	280	**PVX-PVY**	47	1.46E-02
		PVX	43	6.09E-04
		PVY	14	8.64E-04
Cellular component				
Plastid	200	**PVX-PVY**	114	4.38E-55
		PVX	92	2.52E-44
		PVY	20	1.78E-09
Thylakoid	83	**PVX-PVY**	56	1.82E-32
		PVX	49	6.19E-30
		PVY	16	1.24E-11
Extracellular matrix	8	**PVX-PVY**	5	3.77E-03
		PVX	5	9.98E-04
		PVY	5	6.58E-07
Ribosome	250	**PVX-PVY**	43	1.42E-02
		PVX	41	2.08E-04
		PVY	14	3.09E-04
Induced data sets				
Biological process				
Protein metabolism	823	**PVX-PVY**	196	7.46E-19
		PVX	109	6.98E-06
		PVY	55	1.02E-06

(continued on next page)

[a] Gene ontology (GO) categories identified as enriched among the repressed and induced data sets derived from plants inoculated with *Potato virus X* (PVX), *Potato virus Y* (PVY), or PVX and PVY (PVX–PVY). The numbers of EST belonging to each category are reported for the differentially expressed EST and for the EST present in the TIGR microarray. Over-represented GO categories are in bold; *P* = false discovery rate-corrected *P* value for the hypergeometric test.

ment. Thus, the repression of plastid-related genes by the synergistic viral infection was mostly directed against nuclear-encoded genes.

The PVX–PVY synergistic interaction differentially induced the expression of 16 (40%) and 27 (23%) EST classified in response to biotic stimulus and response to stress categories, respectively. Many of the EST within the response to biotic stimulus category were also categorized into the response to stress category. Genes in these categories comprise pathogenesis- or stress-related proteins (including heat-shock proteins and water-deficit response genes), mitogen-activated protein kinases (MAPK) (wound-induced protein kinase [*WIPK*] and salicylic acid-induced protein kinase [*SIPK*]), and enzymes implicated in the biosynthesis of plant oxylipins, among others (Supplementary Table S6). Again, the fold change of most induced genes in response to PVX–PVY infection was greater than the corresponding response to either PVX or PVY. It is noteworthy that these two categories were also overrepresented in the set of EST uniquely induced by PVX–PVY (data not shown).

Comparative analysis of virus infections using MapMan metabolic pathway annotator.

We realized that comparable global results were obtained when our data sets comprising all EST significantly altered by each virus treatment were categorized by using MapMan ontology (Supplementary Table S7). The photosynthesis-related bins showed the most significant changes in terms of average expression profile compared with all the other remaining bins, followed by stress, protein metabolism (synthesis and degradation), lipid metabolism, and carbohydrate metabolism (Wilcoxon rank sum test, $P < 0.05$). The virus treatment that conferred the lowest P values in all these bins was PVX–PVY. Among the set of EST uniquely induced by PVX–PVY and included in the stress biotic subbin (20.1) was one encoding for a plasma membrane–located NADPH-dependent oxidase (BQ508989) (Yoshioka et al. 2003), the respiratory burst oxidase homolog B (*RBOHB*) (two-fold induction). This gene has an incomplete GO annotation in the TIGR potato array and, thus, was not retrieved by BiNGO analysis as classified in the response to stress category.

In virus-infected plants, protein activities are often altered through posttranslational modifications such as ubiquitination (Culver and Padmanabhan 2007). Several subbins associated with protein degradation (bin 29.5) were found to be significantly differentially regulated by either PVX–PVY or PVX infection in MapMan ($P < 0.05$). However, statistically significant overrepresentation of induced genes within protein degradation ($P < 0.0005$, Fisher's exact test) and protein degradation ubiquitin ($P < 0.0001$) subbins was observed only for PVX–PVY. The 72 (19% of total in the array) upregulated genes asso-

Table 1. (*conitnued from previous page*)

Description	No. of total EST	Virus	No. of expressed EST	*P*
Protein biosynthesis	358	**PVX-PVY**	84	6.08E-08
		PVX	35	3.69E-01
		PVY	6	1.00E+00
Cell organization and biogenesis	223	**PVX-PVY**	44	4.90E-03
		PVX	23	3.56E-01
		PVY	4	1.00E+00
Carbohydrate metabolism	168	**PVX-PVY**	44	7.82E-06
		PVX	24	4.12E-02
		PVY	17	1.60E-04
Generation of precursor metabolites and energy	186	**PVX-PVY**	41	8.83E-04
		PVX	23	1.19E-01
		PVY	16	1.59E-03
Response to biotic stimulus	40	**PVX-PVY**	16	6.72E-05
		PVX	6	3.15E-01
		PVY	2	9.16E-01
Response to stress	117	**PVX-PVY**	27	3.95E-03
		PVX	15	1.90E-01
		PVY	8	1.22E-01
Molecular function				
Structural molecule activity	280	**PVX-PVY**	65	3.40E-06
		PVX	27	4.34E-01
		PVY	2	1.00E+00
Translation regulator activity	92	**PVX-PVY**	41	7.57E-13
		PVX	32	2.36E-11
		PVY	8	3.89E-02
Transporter activity	273	**PVX-PVY**	55	9.66E-04
		PVX	45	8.43E-05
		PVY	14	1.75E-01
Protein binding	383	**PVX-PVY**	66	1.44E-02
		PVX	45	5.45E-02
		PVY	23	1.18E-02
Hydrolase activity	831	**PVX-PVY**	127	3.03E-02
		PVX	88	5.02E-02
		PVY	45	1.35E-03
Cellular component				
Ribosome	250	**PVX-PVY**	62	6.16E-07
		PVX	24	4.60E-01
		PVY	0	NA
Cytosol	90	**PVX-PVY**	25	3.97E-04
		PVX	11	3.15E-01
		PVY	4	7.25E-01
Mitochondrion	88	**PVX-PVY**	24	7.08E-04
		PVX	18	2.55E-03
		PVY	7	8.58E-02

ciated with protein degradation ubiquitin subbin encode subunits of the 20S core proteasome, AAA-ATPase and non-ATPase subunits of the 26S proteasome, E2 ubiquitin-conjugating enzymes, E3 ubiquitin-protein ligases, polyubiquitin, and an ubiquitin extension protein, as well as SUMO-conjugating enzymes. These findings suggest that PVX–PVY infection can modulate the proteasome pathway.

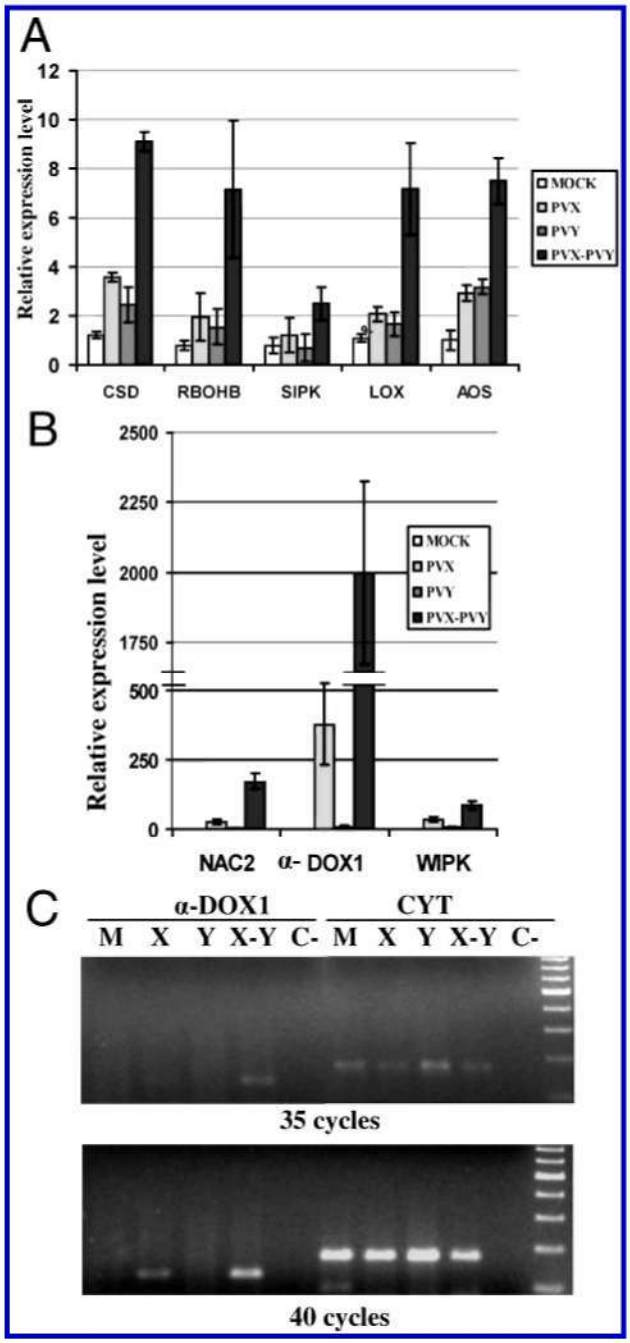

Fig. 3. Comparison of gene expression levels estimated by quantitative reverse-transcriptase polymerase chain reaction (QRT-PCR) and by semiquantitative RT-PCR. RNA samples used for microarray analyses were used in QRT-PCR to determine the relative expression levels of the **A,** superoxide dismutase (*CSD*), respiratory burst oxidase homolog B (*RBOHB*), salicylic acid-induced protein kinase (*SIPK*), 9-lipoxygenases (*9-LOX*), and Allene oxide synthase (*AOS*); and **B,** NAC domain protein NAC2 (*NAC2*), α-dioxygenase1 (*α-DOX1*), and wound-induced protein kinase (*WIPK*) genes in plants inoculated with *Potato virus X* (PVX), *Potato virus Y* (PVY), or PVX and PVY (PVX–PVY), and mock-inoculated plants. Samples were normalized to expression of *Actin* and Cytochrome P450 monooxygenase (*CYT*) gene transcripts. **C,** Relative expression levels of *α-DOX1* mitochondrial RNA using semiquantitative RT-PCR and *CYT* gene transcripts as a control. C is no RT control. Numbers below each panel indicate the number of PCR cycles.

Confirmation of a differential stress response in plants doubly infected by PVX and PVY.

Differential expression of a subset of stress-associated genes was confirmed by real-time quantitative RT-PCR (QRT-PCR) using the same RNA preparations analyzed in microarray ex-

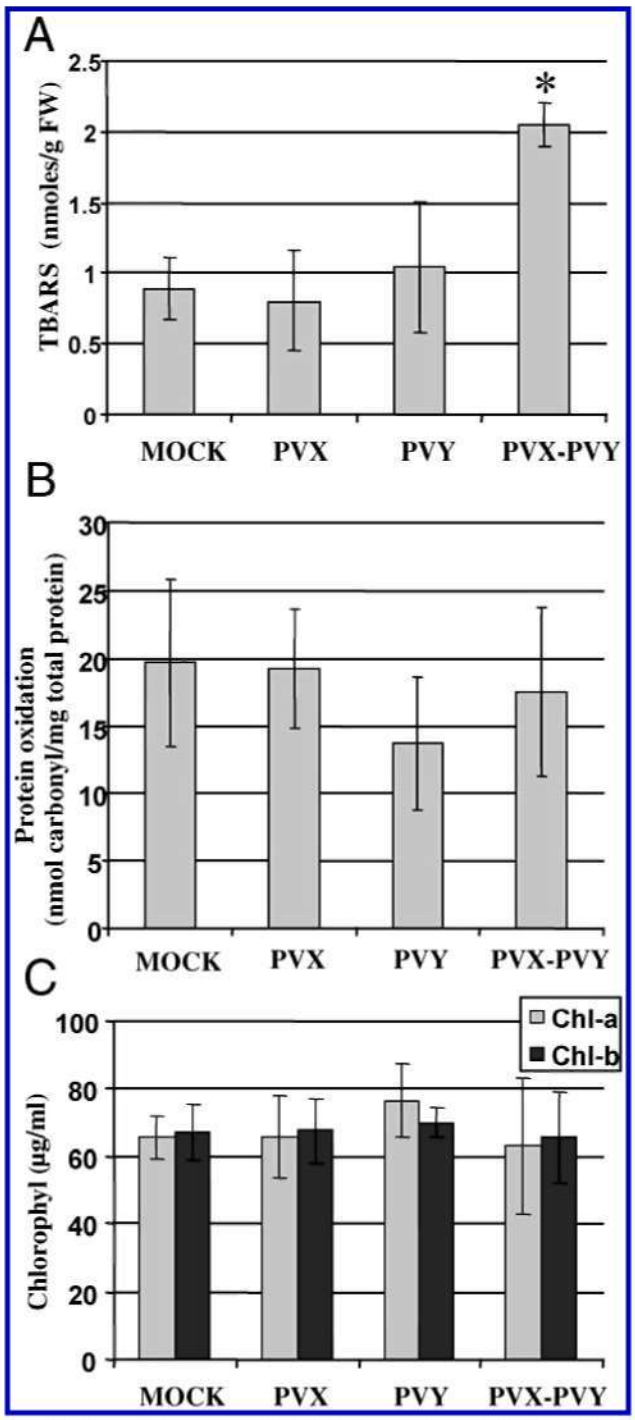

Fig. 4. Effects of *Potato virus X* (PVX), *Potato virus Y* (PVY), or double PVX and PVY (PVX–PVY) infection on **A,** lipid peroxidation (measured as thiobarbituric acid-reactive substances [TBARS]); **B,** protein oxidation (measured as carbonyl-proteins); and **C,** chlorophyll *a* and *chl b* content in *Nicotiana benthamiana* plants at early stages of infection (7 days postinoculation). Data represent the means ± standard errors of at least three replicates. Differences from control values were significant at $P < 0.05$ (*) according to Duncan's multiple range test.

periments. As an independent validation of the microarray results, QRT-PCR experiments with RNA extracted from a new set of inoculated plants (not used for microarray experiments) were repeated with similar results. The relative accumulation of the mRNAs from *RBOHB*, α-dioxygenase1 (*α-DOX1*), superoxide dismutase (*CSD*), *WIPK*, *SIPK*, and an NAC domain protein NAC2 (*NAC2*) was greater in response to PVX–PVY infection compared with PVX or PVY infection, although the absolute values determined by QRT-PCR were higher than those derived from microarray data (Fig. 3). This variation is commonly observed in validation of microarray results by QRT-PCR (Dardick 2007) and is probably due to intrinsic differences between both techniques. Differential induction of *α-DOX1* by PVX–PVY was confirmed by semi-quantitative RT-PCR (Fig. 3C).

An increase in lipid peroxidation and protein oxidation, as well as an imbalance in the antioxidative system of the plant, are oxidative stress parameters commonly associated with susceptible virus–host interactions (Díaz-Vivancos et al. 2008). An oxidative stress was produced in upper, noninoculated leaves of plants infected by PVX–PVY at 7 dpi, as reflected by the 2.3-fold increase in lipid peroxidation compared with mock-inoculated plants (Fig. 4A) (Duncan test, $P < 0.05$). The levels of lipid peroxidation were not significantly altered by either PVX or PVY infection. According to these findings, PVX–PVY infection differentially regulated ($P < 0.05$, Fisher's exact test) the antioxidative system of the plant (redox bin), as revealed by MapMan analysis of microarray data. There was a greater up- or downregulation in the expression of glutathione reductases, catalases, superoxide dismutases, thioredoxins, ascorbate oxidases, and glutathione S-transferases in response to PVX–PVY when compared with single infections (Supplementary Table S8). By contrast, no increase in protein oxidation was observed in PVX–PVY-infected leaves (Fig. 4B).

From the previous results, one can predict that the synergism in pathology caused by PVX–PVY in *N. benthamiana* is in association with the presence or accumulation of reactive oxygen species (ROS). To monitor ROS generation and cell damage in plants infected with the different viruses, superoxide (O_2^-) production and necrosis formation in upper, noninoculated leaves were determined at 7 dpi by staining with nitroblue tetrazolium (NBT) and trypan blue, respectively. Plants inoculated with PVX–PVY exhibited numerous micronecroses predominantly located in periveinal regions of the leaves (Fig. 5A). In contrast, a faint and negligible cell death response was observed in leaves of plants following infection by either PVX or PVY. Consistent with these results, infection by PVX–PVY resulted in strong microoxidative bursts detected by NBT staining (Fig. 5B). However, in plants infected with either PVX or PVY little staining was seen. Upon reduction by O_2^-, NBT forms an insoluble precipitate visualized as a dark-blue-colored formazan deposit. As a result, O_2^- can be detected in vivo and in situ at subcellular levels using this method. Examination under the microscope revealed that the dark-blue-colored formazan precipitates were mostly located in the chloroplasts, revealing a major site of ROS generation (Fig. 5C). This observation indicates that alterations in the chloroplastic metabolism are produced in the early host response to PVX–PVY infection.

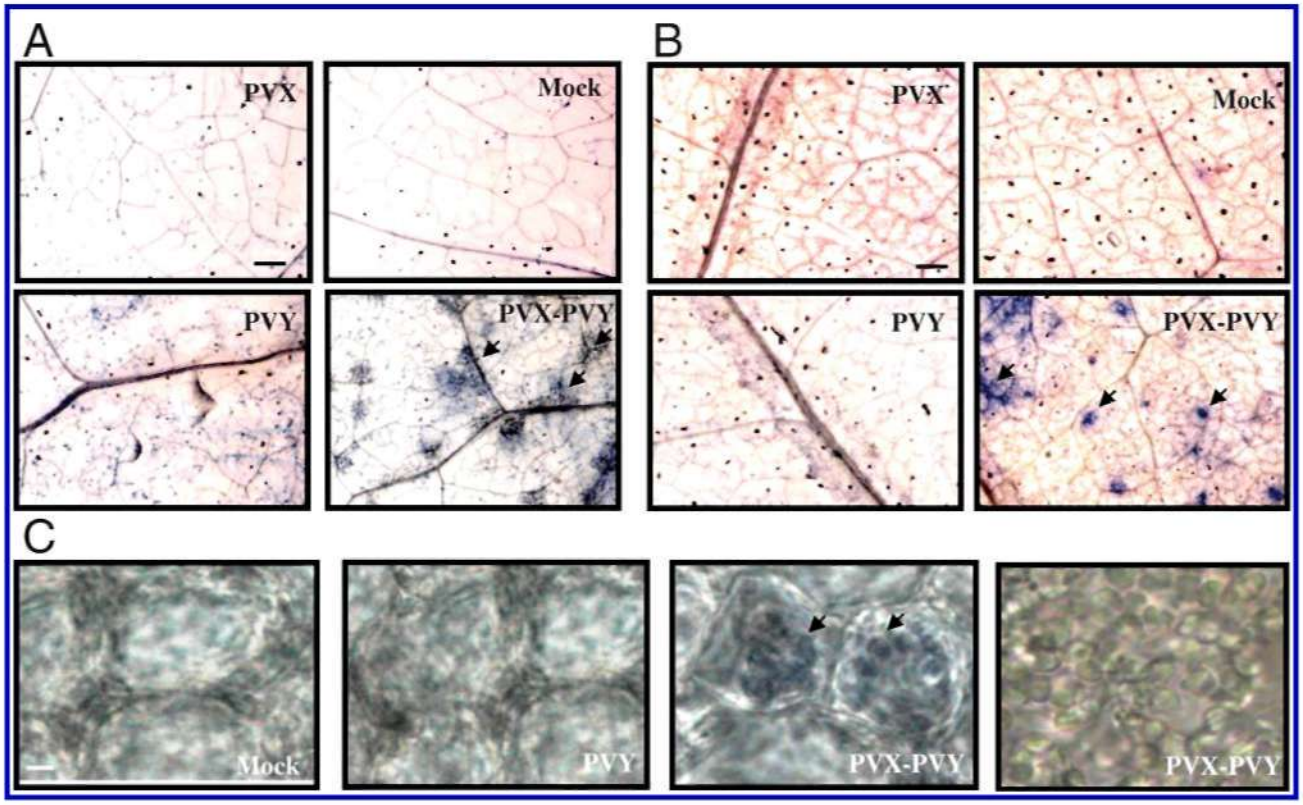

Fig. 5. Micronecrosis and O_2^- generation in systemic leaves of *Nicotiana benthamiana* plants doubly inoculated with *Potato virus X* (PVX) and *Potato virus Y* (PVY) at early stages of infection. **A,** Leaf disks from plants inoculated with PVX, PVY, or PVX and PVY (PVX–PVY), and mock-inoculated plants, were stained with trypan blue at 7 days postinoculation (dpi). After disks had been boiled in ethanol (96%) for 10 min to remove chlorophyll, cell death sites could be visualized as a dark coloration in the PVX–PVY sample. **B,** Leaf disks from plants inoculated with the different virus treatments and mock-inoculated plants were stained with nitroblue tetrazolium (NBT) solution at 7 dpi. O_2^- production could be visualized as dark blue coloration in the PVX–PVY sample. The images were taken at ×15 magnification. Bars = 0.5 mm. **C,** O_2^- produced by PVX–PVY infection originates mostly from chloroplasts. NBT-stained leaf disks were examined under a microscope. The images were taken at ×400 magnification. No reduced dark-blue-colored formazan deposits were observed in chloroplasts of plants inoculated with PVY or PVX (*not shown*) or mock inoculated. To visualize chloroplasts, a partially distained leaf disk is shown in the right panel. Arrows indicate microbursts and micronecrosis. Bar = 20 μm.

It has been suggested that leaf senescence may be a consequence of cumulative membrane deterioration due to increasing levels of lipid peroxidation in chloroplasts (Thompson et al. 1998). Therefore, we aimed to determine whether the double infection-induced accumulation of O_2^- in chloroplast altered the chlorophyll content (an indicator of senescence) of the leaves at the early stages of the synergistic infection. The chlorophyll *a* and *chl b* content of the top leaves of PVX–PVY-infected plants at 7 dpi was not significantly different from that in the corresponding leaves of mock-inoculated plants or plants inoculated with either PVX or PVY (Fig. 4C) (Duncan test, $P > 0.05$). Thus, O_2^- production and the broad downregulation observed for nuclear-encoded genes associated with chloroplastic metabolism in PVX–PVY-infected plants were not correlated with a decay in chlorophyll content at the early stages of the synergistic infection.

PVX–PVY induces the oxylipin biosynthesis pathway.

Further detailed analysis of MapMan diagrams and statistics identified the jasmonic acid (JA) synthesis pathway (bin 17.7.1) as a category of genes differentially regulated by PVX–PVY (Wilcoxon rank sum test, $P < 0.05$) but not by PVX or PVY infection. All these induced genes are predicted to encode a range of enzymes implicated in the biosynthesis of plant oxylipins, a group of oxygenated fatty acid derivatives that play various roles in plant biology (Blée 2002). These genes were represented by one or multiple EST on the array and included 9- and 13-lipoxygenases (*LOX*) (Bannenberg et al. 2009), divinyl ether synthase (*DES*) and 12-oxophytodienoate reductase1 (*OPR1*) (Fig. 6). This set of EST was classified by BiNGO analysis in the GO category response to biotic stimulus. In addition, *α-DOX1*, which is involved in the oxygenation of fatty acids into reactive 2-hydroperoxides (de León et al. 2002), was detected by BiNGO to be present uniquely in the set of EST induced by PVX–PVY. This gene was not categorized into the JA synthesis pathway in MapMan ontology. Overall, the overrepresentation of oxylipin genes in the induced gene set from PVX–PVY infection was statistically significant (Fisher's exact test, $P < 0.0005$). Of 19 EST linked to this category and represented in the potato array, 10 were induced by PVX–PVY, whereas only 1 and 2 EST were induced by PVY and PVX, respectively. QRT-PCR analyses further confirmed that the expression of the oxylipin biosynthesis genes, *9-LOX* and allene oxide synthase (*AOS*), was differentially induced by PVX–PVY (Fig. 3A), even at the very early stages of the infection process (5 dpi) when no cell death response was observed by trypan blue staining (data not shown). Searches in array data sets for enzymes potentially involved in release of unsaturated fatty acids from membranes identified phospholipase Dα1 (BQ505334) (Turner et al. 2002) and phospholipase A_2 (BQ519369) (Dhondt et al. 2000) as genes uniquely induced by PVX–PVY (Fig. 6). No other plant hormone or growth regulator biosynthesis pathway (ethylene, auxin, abscisic acid, salicylic acid, and so on) was differentially expressed in the data sets from any of the three virus infections.

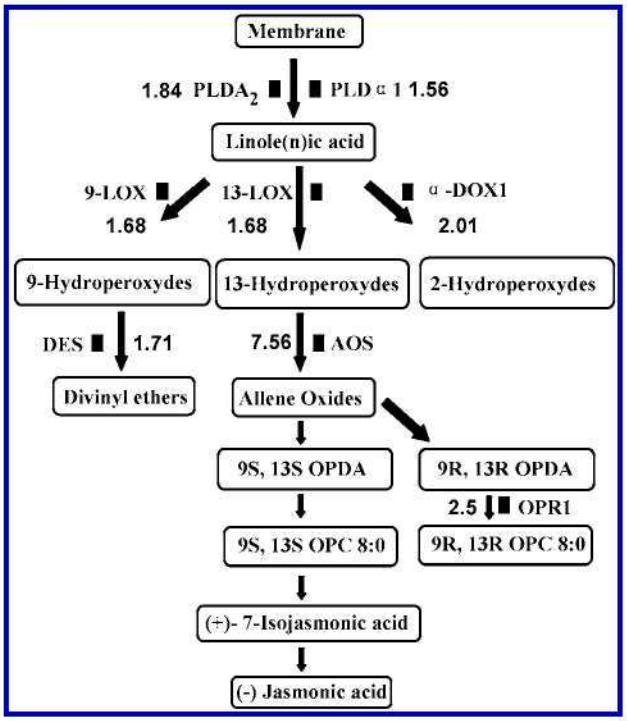

Fig. 6. MapMan illustration of microarray data showing the oxylipin biosynthesis genes which are induced by double infection with *Potato virus X* (PVX) and *Potato virus Y* (PVY) in *Nicotiana benthamiana*. Genes that are represented include phospholipase Dα1 (*PLDα1*), phospholipase A_2 (*PLDA*$_2$), 9- and 13-lipoxygenases (*LOX*), α-dioxygenase1 (*α-DOX1*), divinyl ether synthase (*DES*), allene oxide synthase (*AOS*), and 12-oxophytodienoate reductase1 (*OPR1*). The values represent the fold changes from microarray expression data, except for *AOS*, which was obtained from quantitative reverse-transcriptase polymerase chain reaction (QRT-PCR). Because *α-DOX1* and *OPR1* are represented in the induced data set by more than one expressed sequence tag (EST), the mean fold change values for these genes are given. 9S, 13S OPDA, and 9R, 13R OPDA = 12-oxophytodienoic acid stereoisomers; 9S, 13S OPC 8:0, and 9R, 13R OPC 8:0 = 3-oxo-2(2′(Z)-pentenyl)-cyclopentane-1-octanoic acid stereoisomers.

To assess a functional role of oxylipins in the PVX–PVY synergistic disease, VIGS technology was used to inhibit *α-DOX1* gene expression, which represents one of the various biosynthetic branches that lead to oxylipins. The third and fourth true leaves of 4-week-old *N. benthamiana* plants were infiltrated with a mixture of *Agrobacterium* cultures containing pTRV1 and pTRV2-*α-DOX1* constructs, whereas a mixture of Agrobacterium cultures containing pTRV1 and pTRV2 was used as a control. At 7 days after infiltration (dai), plants were either mock inoculated or challenge inoculated with PVX, PVY, or the PVX–PVY combination in upper, noninfiltrated leaves. The *α-DOX1* mRNA was substantially less abundant in the uppermost leaves from pTRV2-*α-DOX1* plants than in the corresponding leaves from pTRV2-infiltrated plants at 7 dpi with the PVX–PVY pair (14 dai) (Fig. 7A). Expression of a few selected genes that were significantly up- or downregulated in doubly infected plants (Fig. 3) was analyzed by QRT-PCR in *α-DOX1*-silenced plants infected with PVX–PVY. *AOS, CSD, RBOHB, SIPK*, and *HCF136* mRNAs were present at equivalent levels in silenced and control, pTRV2-infiltrated plants ($F_{1,17} < 6.81$, $P > 0.01$). Suppression of *α-DOX1* expression in mock-inoculated, pTRV2-*α-DOX1*-infiltrated plants had no visible effects on plant growth or development.

Typical disease symptoms developed simultaneously in silenced and nonsilenced plants singly infected with either PVX or PVY and viral titers reached similar levels in both groups of plants (data not shown). Systemic mosaic symptoms developed at 6 dpi in both pTRV2-*α-DOX1*- and pTRV2-infiltrated plants that were challenge inoculated with PVX–PVY. Ten days after inoculation, the pTRV2-infiltrated plants began to exhibit the necrosis symptoms typical of the viral synergistic interaction. In contrast, *α-DOX1*-silenced plants exhibited only strong mosaic symptoms with no visible response of necrosis at this time point (Fig. 7B). Eventually, *α-DOX1*-silenced plants showed systemic necrosis and death afterward. Consistent with these observations, trypan blue staining at 7 dpi revealed that many cell death sites were located in periveinal regions in the uppermost leaves of pTRV2-infiltrated plants (Fig.

7C). However, pTRV2-*α-DOX1*-infiltrated plants displayed significantly reduced area and intensity of staining, suggesting that delayed cell death happened in *α-DOX1*-silenced leaf tissue during PVX–PVY infection. These same results were obtained in each of three repeated tests with 5 plants each. Northern blot and RT-PCR analyses confirmed that the level of accumulation of PVX RNA and PVY RNA at 10 dpi was similar in both group of plants, ruling out the possibility that the delayed cell death was due to limited virus spread or accumulation in *α-DOX1*-silenced plants (Fig. 7D and E). Lipid peroxidation was still found at greater levels in silenced plants infected with PVX–PVY compared with mock-inoculated controls (data not shown), suggesting that *α-DOX1* activity is not the main contributor to lipid peroxidation in PVX–PVY synergism.

DISCUSSION

Infection of plants by multiple viruses is a common phenomenon in nature, with unpredictable pathological consequences. The present study shows the use of microarray techniques for the monitoring of changes in gene expression induced by the best-studied synergistic pair, PVX and PVY.

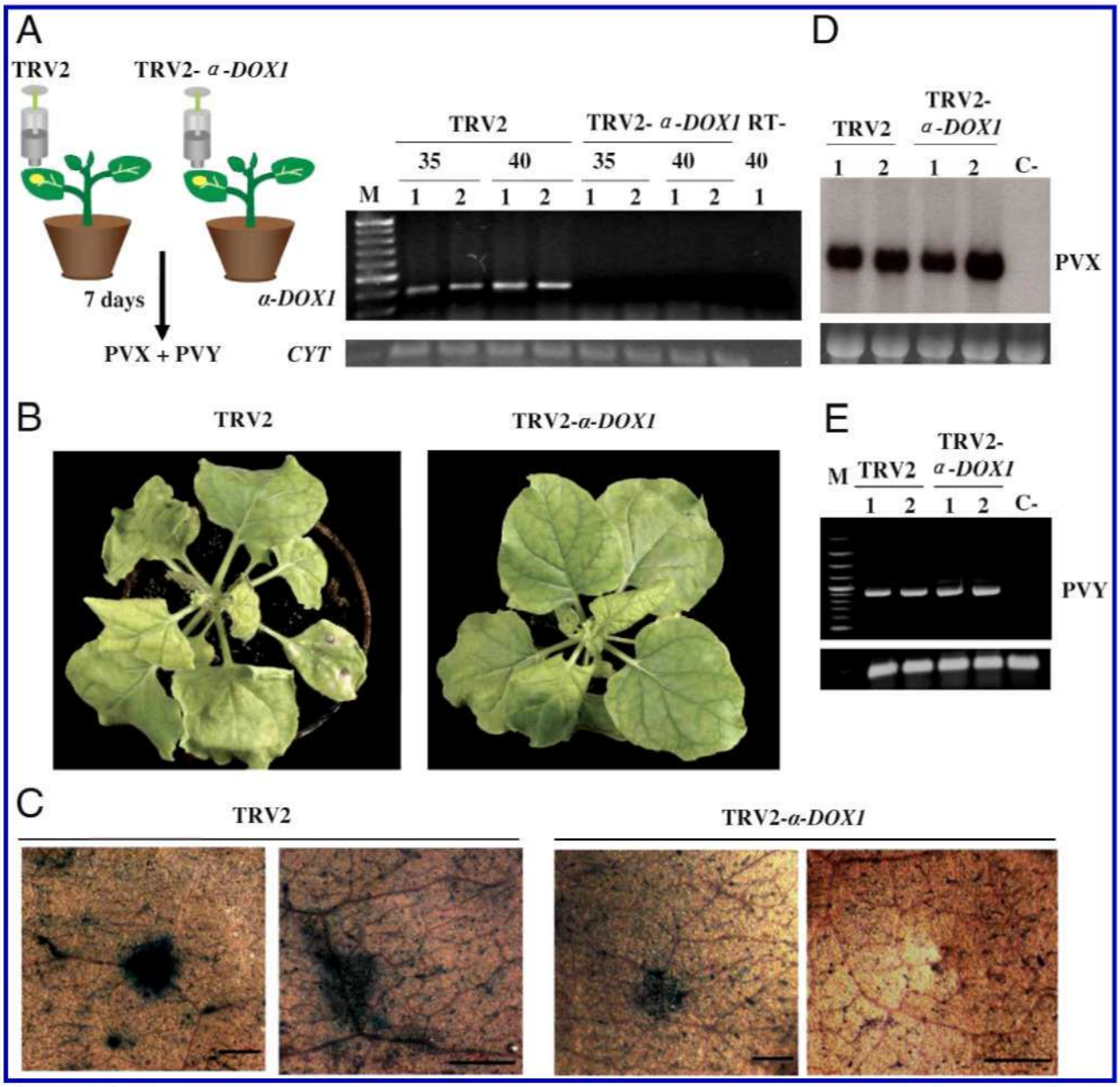

Fig. 7. Effect of α-dioxygenase1 (*α-DOX1*) silencing on *Potato virus X* (PVX)–*Potato virus Y* (PVY) infection. **A,** Plants were infiltrated with *Agrobacterium* cultures containing a 1:1 mixture of pTRV1 and pTRV2 (as a control) or pTRV1 and pTRV2-*α-DOX1*. At 7 days after infiltration (dai), plants were inoculated with PVX and PVY in upper leaves. Silencing of *α-DOX1* transcripts was monitored by reverse-transcriptase polymerase chain reaction (RT-PCR) in uppermost leaves from two individuals per treatment at 7 days postinoculation (dpi) with viruses (14 dai). The number of PCR cycles is indicated below treatments. C is no RT control. *CYT* is a loading control. **B,** Representative disease symptoms displayed at 10 dpi. Control plants exhibited the typical necrosis symptoms associated with the viral synergistic interaction, while *α-DOX1*-silenced plants exhibited mosaic symptoms but not necrosis. **C,** Discs from uppermost leaves of control and *α-DOX1*-silenced plants were stained with trypan blue to detect cell death at 7 dpi with PVX and PVY (14 dai). The images were taken at ×20 (first and third panel) and ×30 (second and fourth panel) magnification. Bars = 0.5 mm. **D,** Northern blot hybridization showing PVX RNA accumulation in control and *α-DOX1*-silenced plants at 10 dpi using PVX coat protein (CP) sequences as a probe. Ethidium bromide-stained RNA is shown as loading control. **E,** RT-PCR amplification of PVY CP gene in control and *α-DOX1*-silenced plants at 10 dpi. The same RT reactions were used to amplify Actin gene transcripts as a control.

Comparative microarrays using singly and doubly infected *N. benthamiana* plants that displayed distinctive symptoms offer unique opportunities to link specific changes in global host gene expression to the increase in virulence which are independent of the dramatic increase in PVX accumulation that is typical of the PVX–PVY synergism in *N. tabacum*.

PVX–PVY infection induced an increase in both the number of host genes that were expressed differentially and the magnitude of the changes compared with infection by PVX or PVY (Fig. 2). This trend was observed over the entire array for most genes that passed our selection criteria (data not shown). Furthermore, the relative proportion of genes uniquely altered by PVX–PVY was greater than the corresponding ones from either PVX or PVY infection. This introduces a qualitative difference in the host response to PVX–PVY infection, which could be responsible, at least in part, for the synergism in pathology. Unique EST that were altered by either PVX or PVY infection could represent genes that displayed compensatory changes in the PVX–PVY infection. Previous experiments showed no differences in the number of cells infected by PVX in single and double infections with PVY in *N. tabacum* (Goodman and Ross 1974); therefore, the hypothesis that a change in the number or type of infected cells was responsible for the greater changes in global gene expression observed in *N. benthamiana* plants infected by PVX–PVY is unlikely. Altogether, these findings suggest a more drastic reprogramming of gene expression in doubly infected cells.

GO enrichment analyses further revealed qualitative and quantitative differences associated with PVX–PVY synergism (Table 1). By using a different statistical approach embedded in MapMan software, nearly identical functional groups of genes were found to be differentially regulated in PVX–PVY infection in terms of their average response versus the response of all the other genes in the data set. These findings suggest that suites of overrepresented genes are expressed coordinately in response to PVX–PVY synergism. Genes modulated by PVX–PVY infection appear to be scattered among several metabolic pathways, confirming that the host response to virus synergism in *N. benthamiana* includes a coordinated rearrangement of a wide array of cellular processes rather than a simple induction of genes involved in stress responses.

PVX–PVY infection uniquely showed widespread induction of protein biosynthesis-related genes, as previously reported in several studies involving single virus infections (Dardick 2007; Yang et al. 2007; Babu et al. 2008). In doubly infected plants, the coordinated upregulation of translation-associated genes may be modulated by the viruses to produce excess machinery and provide the additional resources required to translate the two highly replicating viral RNAs and produce viral proteins. Alternatively, this response may be partially caused by the plant's need to compensate for the loss in its ability to synthesize its own proteins or, perhaps, to induce the expression of genes aimed at a more robust defense response against the double infection. At present, we cannot distinguish between changes in the protein synthesis machinery which are beneficial to viral multiplication and the general stress responses activated by the plant. In this regard, the coordinated induction of genes involved in ubiquitin-dependent protein degradation is noteworthy. This may represent a resistance response to double infection by targeting viral proteins for destruction which, in turn, potentially might alter degradation of specific host factors affecting virus pathogenicity (Culver and Padmanabhan 2007).

Stress-related genes were overrepresented and differentially regulated by PVX–PVY infection, as has been observed in different virus–host combinations (Whitham et al. 2006; Dardick 2007; Babu et al. 2008). However, a role for these defense-like responses in limiting virus spread is controversial (Huang et al. 2005; Love et al. 2005). Nevertheless, stress responses elicited by virus infection in compatible hosts might have an impact on symptom development.

Several studies suggest that differential downregulation of chloroplast-related gene expression is correlated with viral symptoms such as mosaic and chlorosis (Dardick 2007; Yang et al. 2007; Havelda et al. 2008). The overrepresentation of GO categories related to chloroplast function was greater in PVX–PVY compared with single infections which, together with the overall magnitude of repression, was correlated with the severity of the chlorotic symptoms. The increased expression of genes related to carbohydrate metabolism might be linked as well to the synergism in pathology, because appearance of chlorosis in *Cucumber mosaic virus*-infected cucumber has been associated with increased glycolysis and respiration and decreased photosynthetic activity (Técsi et al. 1996). One possible mechanism to account for the deeper repression of chloroplast-associated genes observed in PVX–PVY-infected tissue could be the degradation of plastids themselves as a primary cause of this repression. Although chloroplast degradation cannot be ruled out as an ongoing process, the lack of impact on either chloroplast-encoded genes or chlorophyll content of the leaves and the induction of the oxylipin biosynthesis pathway located predominantly in chloroplasts suggest that chloroplast integrity and some kind of chloroplastic metabolism remain intact at the early stages of the synergistic infection. Alternatively, by impairing photosynthetic activity in chloroplasts through the repression of nuclear-encoded genes, viruses could suppress basal defense mechanisms (Abbink et al. 2002). In this sense, chloroplasts have been reported to be a source of oxidative stress during viral infection (Díaz-Vivancos et al. 2008), actively promoting the generation of ROS (Liu et al. 2007). Accordingly, gene silencing targeted against specific photosystem subunits in virus-infected plants results in a higher viral accumulation in the plant (Abbink et al. 2002). Nevertheless, PVX–PVY produced an oxidative stress in *N. benthamiana*, as reflected by the generation of O_2^- in chloroplasts, the increase in lipid peroxidation, and the induction of O_2^--scavenger genes (e.g., *CSD*). The general repression of photosynthetic metabolism could help the plant to minimize oxidative damage caused by PVX–PVY infection.

Some works have shown that increased levels of ROS could contribute to the development of disease symptoms such as chlorosis, malformations, and growth abnormalities in systemically virus-infected plants (Riedle-Bauer 2000; Díaz-Vivancos et al. 2008). Enhanced chlorotic symptoms observed in plants infected by PVX–PVY could be due to an increased generation of ROS in chloroplast, induced by a disturbance of the photosynthetic electron chain through the observed repression of PSI and PSII subunit mRNAs. In addition, increased levels of enzymes associated with the detoxification of ROS have also been demonstrated in plants undergoing compatible infection with different viruses (Allan et al. 2001; Clarke et al. 2002). Here, we report a differential expression of *RBOHB*, *WIPK*, and *SIPK*, as well as several genes involved in the regulation of redox homeostasis in systemic leaves of PVX–PVY-infected plants, suggesting that ROS signaling constitutes an important part of the host response to virus synergism. In support of this scenario, the plasma membrane-located NADPH oxidase complex (*RBOH*) has been identified as a source of ROS in susceptible *Arabidopsis* plants infected with *Cauliflower mosaic virus* (Love et al. 2005), and *SIPK* as well as *WIPK* are activated by pathogens and oxidative stresses (Zhang et al. 2000; Zhang and Liu 2001). Thus, our experiments suggested that at least two distinct cell compartments, plasma membrane and chloroplast, contribute to the generation of ROS in PVX–PVY-infected plants.

MAPK cascades are known as major pathways by which biotic or abiotic stimuli are transduced into intracellular responses in plants (Asai et al. 2002). The most remarkable symptom caused by PVX–PVY infection was the appearance of large necrotic stripes or lesions occurring on stems and systemically infected leaves. It is likely that progression of micronecroses observed in periveinal regions in the leaves at early stages of infection lead to vascular wilt and collapse of the plant (Fig. 5). The induction of water-deficit response genes revealed by microarray experiments could result from necrosis of the vascular tissue, which likely cuts off water supplies to the lamina of the leaves and causes the observed wilting of the plant. Interestingly, members of the WRKY family of transcription factors, included *WRKY6*, were also significantly induced and overrepresented (Fisher's exact test, $P < 0.0005$) in response to virus synergism (data not shown). This observation is noteworthy, given the ability of WRKY proteins to be induced by activation of the SIPK/WIPK cascade and to mediate cell death processes (Kim and Zhang 2004). Thus, it is tempting to speculate on the involvement of a SIPK/WIPK cascade in the induction of the necrosis triggered by PVX–PVY in *N. benthamiana*. Indeed, recent studies suggest that cell death in different compatible interactions also involves the activation of MAPK cascades (del Pozo et al. 2004). These data highlight the similarity between the signaling pathways triggered in a host plant during successful infection by a necrosis-inducing virus synergism and the resistance responses normally effective against incompatible pathogens.

We present evidence that PVX–PVY infection promotes the peroxidation of lipids (Fig. 4), a marker of stress situations which is often associated with cell death in incompatible interactions. In addition to ROS-mediated lipid peroxidation, enzymatic production of fatty acid hydroperoxides has been observed as a result of lipoxygenase (*9-LOX* and *13-LOX*) and *α-DOX1* activities (Blée 2002). Remarkably, doubly infected plants uniquely showed significant increases in the expression of genes associated with oxylipin production, at both the level of average response and the number of induced genes represented in the potato array. Up- or downregulation of *LOX* mRNA has been reported in different virus–host compatible interactions (Babu et al. 2008). However, coordinated induction of up to seven genes of the oxylipin biosynthesis pathway has not been previously documented. At present, we cannot distinguish between enzymatic oxidation and chemical autoxidation of lipids in our data based on thiobarbituric acid-reactive substances (TBARS) measurements. However, we favor the hypothesis that lipid peroxidation at early stages of the PVX–PVY infection process is produced mainly via enzymatic activities rather than generated by ROS, because no increase in protein oxidation, another oxidative stress parameter promoted by ROS, was observed in doubly infected plants. Previous results minimize the direct participation of ROS from the oxidative burst in membrane lipid peroxidation elicited by the fungal hypersensitive response (HR) elicitor cryptogein in tobacco leaves (Rustérucci et al. 1999).

Oxylipins have important roles in different developmental and physiological processes in plants, as well as in plant defense against pathogens and insects (Blée 2002). Interestingly, a role of several oxylipins originated from *9-* and *13-LOX* activities in promoting localized cell death during the HR has been reported in different pathosystems (Rustérucci et al. 1999; Vollenweider et al. 2000). By contrast, 2- and 9-hydroperoxy fatty acids produced by either *α-DOX1* or *9-LOX* activities were proposed to protect tissues from HR collapse caused by avirulent *Pseudomonas syringae* (de León et al. 2002; Hamberg et al. 2003). In our compatible pathosystem, downregulation of *α-DOX1* gene expression by VIGS led to a delay in the appearance of necrotic symptoms during PVX–PVY infection, which was correlated with an attenuated cell death response at early stages of infection. Such an observation apparently contradicts the proposed cell-death-protecting properties of 2-hydroperoxy fatty acids produced by *α-DOX1* (de León et al. 2002). However, these properties were inferred from experiments with an incompatible bacterium. The impact of α-DOX1 silencing on virus synergism-associated cell death indicates that oxylipins may differentially affect plant responses in distinct host–pathogen interactions. The *α-DOX1*-silenced plants were not less susceptible to systemic infection by PVX–PVY compared with control plants, suggesting that *α-DOX1* does not interfere with successful infection by the synergistic pair.

Although these findings indicated that the oxylipin pathway plays a role in plant death elicited by PVX–PVY synergistic infection in *N. benthamiana*, definite experimental evidence has not yet verified that infection by PVX–PVY and the necrosis response can be uncoupled. Because of the complexity of the oxylipin signaling network (Vellosillo et al. 2007), the functional redundancy of multiple *LOX* genes (Bannenberg et al. 2009), and interactions between the *LOX* and *α-DOX1* pathways (Hamberg et al. 2003), studies of the involvement of the oxylipin pathway in plant death response to virus infections will require knock down of double or multiple enzymes of the pathway rather than targeting single enzymes. Recent studies have shown that induction of JA biosynthesis genes by different stresses involves activation of WIPK/SIPK cascades (Schweighofer and Meskiene 2008); therefore, it will be interesting to examine the role of MAPK upregulated by PVX–PVY in the induction of the necrosis response.

MATERIALS AND METHODS

Virus and inoculations.

N. benthamiana plants were grown in a growth chamber with a cycle of 16 h of light and 8 h of darkness at 25°C. Four-week-old *N. benthamiana* plants were inoculated by rubbing plant sap infected with PVX or PVY onto two fully expanded leaves as described (González-Jara et al. 2004). Control plants were mock inoculated with extracts from healthy leaves and the leaves were harvested at the same time points as the infected plants.

RNA isolation, Northern blot, and RT-PCR analysis.

Total RNA was extracted from upper, noninoculated leaf tissue with Trizol reagent (Invitrogen, San Diego, CA, U.S.A.), followed by purification with RNeasy midiprep columns (Qiagen, Hilden, Germany). Northern blot analysis was done as described by Tenllado and Díaz-Ruíz (2001).

Radiolabeled probes were made by random priming reactions in the presence of α-^{32}P-dCTP. A 299-bp *Sst*I fragment from the *N. plumbaginifolia CAB-E* (M21398) and the 3′-terminal 672-bp fragment of the *N. benthamiana HCF136* genes were used as probes (Tenllado and Díaz-Ruíz 2001). PVX RNA was detected by hybridization with probes corresponding to PVX coat protein (CP) sequences (González-Jara et al. 2004). Densitometry analyses of blots were performed in a calibrated densitometer GS-800 (Bio-Rad Laboratories, Hercules, CA, U.S.A.), using the Quantity One (Bio-Rad) software.

PVY RNA was detected by RT-PCR as described (González-Jara et al. 2004) using the oligonucleotides CP-F and CP-R. The *N. benthamiana Actin* gene transcripts were amplified as an internal control by using the oligonucleotides ACT-F and ACT-R.

Microarray analysis.

Three independent biological replicates were used to monitor differences in gene expression between treatments. For

each biological replicate, three symptomatic, noninoculated upper leaves from each of five plants per treatment or similar-aged healthy leaves from mock-inoculated controls were harvested and immediately frozen in liquid N_2. RNA quantification and RNA quality determination were done as described (Adie et al. 2007). RNA was screened by RT-PCR and Northern blot to ensure that virus-inoculated plants were infected with appropriate viruses.

The TIGR potato microarray contains 11,412 validated cDNA clones (Rensink et al. 2005). Hybridization and scanning of slides was performed in accordance with Adie and associates (2007). The expression data were normalized and statistically analyzed using the LIMMA package (Smyth and Speed 2003). Linear model methods were used for determining differentially expressed genes using an empirical Bayes moderated *t* statistic (Smyth 2004). To control the false discovery rate, P values were corrected using the method of Benjamani and Hochberg (1995). The expected false discovery rate (FDR) was controlled to be <5%. EST were considered to be differentially expressed if $Q < 0.05$. In addition, only genes with a fold change of more than 1.5 (up or down) were considered for further analysis. Statistical analysis at either 1 or 5% FDR with no fold-change cut-off gave qualitatively identical results, confirming their robustness to changes in arbitrarily chosen statistical thresholds. The expression profiles resulting from different treatments were grouped based on similarity in pattern of their expression by using hierarchical cluster analysis based on Euclidean distance and complete linkage (MeV TIGR software).

Overrepresentation analysis.

BiNGO (Maere et al. 2005) was used to determine which GO terms were significantly over and underrepresented in the sets of statistically significant EST induced or repressed for each virus treatment using the hypergeometric test. The plant-specific GO Slim process, component, and function ontologies were used. The EST for which there were no GO annotations in the TIGR potato array were not recognized in the test or reference set by BiNGO and, thus, were not taken into account in the overrepresentation analysis. Only GO terms with corrected *P* values < 0.05 (Benjamani and Hochberg 1995) were considered to be overrepresented in our analysis.

The list of EST that were statistically altered by each virus infection was imported into the MapMan visualization software (Thimm et al. 2004), which allows microarray data to be plated on any known plant metabolic pathway or process. A Wilcoxon rank sum test implemented in MapMan was used to extract functional groups (bins) whose members exhibited a significantly different regulation compared with all other remaining bins in the data set (Benjamani and Hochberg corrected *P* value < 0.05). Fisher's exact test was used to test for significant overrepresentation of the number of genes within the MapMan bins.

A list of the 43 potato EST represented in the TIGR array that matched 26 *Arabidopsis* chloroplast-encoded genes (BLASTN *E* value < e-10) was obtained from C. Dardick (*personal communication*).

Detection of oxidative stress parameters and chlorophyll quantification.

In vivo O_2^- generation was detected in disks detached from systemic leaves at 7 dpi using NBT staining as described (Díaz-Vivancos et al. 2008). Leaf disks were stained with lactophenol-trypan blue as described (Hamberg et al. 2003). Representative phenotypes were photographed with a Leica L2 stereoscope and Leica DM 2500 microscope using a Leica DFC 320 camera.

Chlorophyll *a* and *chl b* measurements were done according to Inskeep and Bloom (1985). Leaf disks (5 mm in diameter) were excised from different areas of systemically infected leaves and pooled in triplicate. Discs were homogenized by means of a plastic pestle in 1 ml of 80% acetone. Extracts were diluted 10-fold in 100% acetone and A647 and A664 were measured. Relative chlorophyll levels were expressed as micrograms of chlorophyll per milliliter. Lipid peroxidation was estimated by determining the concentration of TBARS, as described previously (Hernández and Almansa 2002). The absorbance of the samples was read at 532 nm. The value for nonspecific absorption at 600 nm was subtracted. The amount of TBARS was calculated from the extinction coefficient 155 mM^{-1} cm^{-1}. The carbonyl content in oxidatively modified proteins was quantified using the 2,4-dinitrophenylhydrazone assay procedure (Levine et al. 1990). At least two independent experiments were conducted in each case, with three to six replicates for each treatment. Statistical analyses (analysis of variance followed by Duncan's multiple range test) were performed using the statistical software STATGRAPHICS Plus 5.1 (Statistical Graphics Corp., Princeton, NJ, U.S.A.).

QRT-PCR analysis.

QRT-PCR reactions were performed in the iCycler iQ5 real-time PCR detection system (Bio-Rad). One-step RT-PCR was performed using total RNA preparations treated with TURBO DNase (Ambion, Austin, TX, U.S.A.). The real-time assay was performed using 15 µl of a reaction mix that contained 7.5 µl of Biotools QuantiMix EASY SYG (Biotools, Madrid, Spain), 2.5 µl of RNase-free water, 0.075 µl of MuLV reverse transcriptase, 0.075 µl of RNase Inhibitor, 0.3 µM each primer, and 3 µl of total RNA extract (RNA at approximately 10 ng/µl). Real-time RT-PCR with and without reverse transcriptase were run in parallel to ensure the absence of DNA template in the samples. All reactions were done in triplicate and the values obtained averaged. QRT-PCR was carried out at 48°C for 30 min; 95°C for 10 min; and 40 cycles of 95°C for 30 s, 64°C for 30 s, and 72°C for 20 s. Synthesis of cDNA products of approximately 150 bp in length was confirmed by melting curve analysis using the iQ5 software. Both Actin and Cytochrome P450 monooxygenase (*CYT*) genes were chosen for normalization because of their similar level of expression across all virus infections and their PCR amplification efficiencies. All cDNA products were sequenced to confirm their identity.

VIGS.

A 466-bp cDNA fragment corresponding to the 3′ part (nucleotides 1,364 to 1,829) of *α-DOX1* from *N. tabacum* (de León et al. 2002) was amplified by PCR using oligonucleotides DOX1-F1 and DOX1-R1, subsequently cut with *Bam*HI and *Xho*I, and ligated into the binary vector pTRV2 to yield pTRV2-α-DOX1 (Liu et al. 2002). The pTRV1 vector and the pTRV2 vector with or without *α-DOX1* were transformed into *Agrobacterium tumefaciens* 2260. *N. benthamiana* leaves were infiltrated with *A. tumefaciens* cultures as described (Tenllado and Díaz-Ruíz 2001).

α-DOX1 mRNA was detected by RT-PCR as described (Liu et al. 2002). The following thermal cycle conditions were used: 94°C for 4 min, followed by 94°C for 30 s, 55°C for 30 s, and 72°C for 30 s for 30, 35, 40, and 50 cycles. Because 35 and 40 cycles of amplification were within the log-linear phase of PCR product amplification in the nonsilenced control sample, these conditions were selected for comparison of relative accumulation of *α-DOX1* mRNA in all samples. Primers DOX1-F2 and DOX1-R2 that anneal outside the region targeted for silencing were used to ensure that only the endogenous gene was being tested. The *CYT* gene transcripts were amplified as an internal control by using the oligonucleotides CYT-F and CYT-R.

ACKNOWLEDGMENTS

A. García-Marcos was recipient of a contract from the Consejo Superior de Investigaciones Científicas (CSIC) and R. Pacheco was recipient of a predoctoral I3P fellowship from the CSIC. This work was supported by grant BIO2006-10944 from the Ministerio Educacione y Ciencia and by grant 200540M109 from the Comunidad Autónoma de Madrid. We thank C. Castresana for providing the cDNA clone of *α-DOX1*, S. P. Dinesh-Kumar for providing the TRV system, C. Dardick for sharing unpublished data, J. A. Hernández for advice in oxidative stress measurements, C. Llave and T. Canto for comments on the manuscript, and M. García for technical assistance.

LITERATURE CITED

Abbink, T. E., Peart, J. R., Mos, T. N., Baulcombe, D. C., Bol, J. F., and Linthorst, H. J. 2002. Silencing of a gene encoding a protein component of the oxygen-evolving complex of photosystem II enhances virus replication in plants. Virology 295:307-319.

Adie, B. A., Pérez-Pérez, J., Pérez-Pérez, M. M., Godoy, M., Sánchez Serrano, J. J., Schmelz, E. A., and Solano, R. 2007. ABA is an essential signal for plant resistance to pathogens affecting JA biosynthesis and the activation of defenses in *Arabidopsis*. Plant Cell 19(5):1665-1681.

Allan, A. C., Lapidot, M., Culver, J. N., and Fluhr, R. 2001. An early *Tobacco mosaic virus*-induced oxidative burst in tobacco indicates extracellular perception of the virus coat protein. Plant Physiol. 126:97-108.

Asai, T., Tena, G., Plotnikova, J., Willmann, M. R., Chiu, W. L., Gomez-Gomez, L., Boller, T., Ausubel, F. M., and Sheen, J. 2002. MAP kinase signalling cascade in *Arabidopsis* innate immunity. Nature 415:977-983.

Babu, M., Gagarinova, A. G., Brandle, J. E., and Wang, A. 2008. Association of the transcriptional response of soybean plants with *Soybean mosaic virus* systemic infection. J. Gen. Virol. 89(4):1069-1080.

Bannenberg, G., Martínez, M., Hamberg, M., and Castresana, C. 2009. Diversity of the enzymatic activity in the lipoxygenase gene family of *Arabidopsis thaliana*. Lipids 44(2):85-95.

Benjamani, Y., and Hochberg, Y. 1995. Controlling the false discovery rate. J. R. Stat. Soc. (Ser. A) 57:289-300.

Blée, E. 2002. Impact of phyto-oxylipins in plant defense. Trends Plant Sci. 7:315-321.

Clarke, S. F., Guy, P. L., Burritt, D. J., and Jameson, P. E. 2002. Changes in the activities of antioxidant enzymes in response to virus infection and hormone treatment. Physiol. Plant. 114:157-164.

Culver, J. N., and Padmanabhan, M. S. 2007. Virus-induced disease: Altering host physiology one interaction at a time. Annu. Rev. Phytopathol. 45:221-243.

Dardick, C. 2007. Comparative expression profiling of *Nicotiana benthamiana* leaves systemically infected with three fruit tree viruses. Mol. Plant-Microbe Interact. 20:1004-1017.

de León, I. P., Sanz, A., Hamberg, M., and Castresana, C. 2002. Involvement of the *Arabidopsis* α-DOX1 fatty acid dioxygenase in protection against oxidative stress and cell death. Plant J. 29:61-72.

del Pozo, O., Pedley, K. F., and Martin, G. B. 2004. MAPKKKalpha is a positive regulator of cell death associated with both plant immunity and disease. EMBO (Eur. Mol. Biol. Organ.) J. 23:3072-3082.

Dhondt, S., Geoffroy, P., Stelmach, B. A., Legrand, M., and Heitz, T. 2000. Soluble phospholipase A2 activity is induced before oxylipin accumulation in *Tobacco mosaic virus*-infected tobacco leaves and is contributed by patatin-like enzymes. Plant J. 23:431-440.

Díaz-Vivancos, P., Clemente-Moreno, M J., Rubio, M., Olmos, E., García, J. A., Martínez-Gómez, P., and Hernández, J. A. 2008. Alteration in the chloroplastic metabolism leads to ROS accumulation in pea plants in response to plum pox virus. J. Exp. Bot. 59(8):2147-2160.

González-Jara, P., Tenllado, F., Martínez-García, B., Atencio, F. A., Barajas, D., Vargas, M., Díaz-Ruiz, J., and Díaz-Ruiz, J. R. 2004. Host-dependent differences during synergistic infection by Potyviruses with potato virus X. Mol. Plant Pathol. 5:29-35.

González-Jara, P., Atencio, F. A., Martínez-García, B., Barajas, D., Tenllado, F., and Díaz-Ruiz, J. R. 2005. A single nucleotide mutation in the *Plum pox virus* HC-Pro gene abolishes both synergistic and silencing suppression activities. Phytopathology 95:894-901.

Goodin, M. M., Zaitlin, D., Naidu, R. A., and Lommel, S. A. 2008. *Nicotiana benthamiana*: Its history and future as a model for plant-pathogen interactions. Mol. Plant-Microbe Interact. 21:1015-1026.

Goodman, R. M., and Ross, A. F. 1974. Enhancement of potato virus X synthesis in doubly infected tobacco occurs in doubly infected cells. Virology 58:16-24.

Hamberg, M., Sanz, A., Rodriguez, M. J., Calvo A. P., and Castresana, C. 2003. Activation of the fatty acid α-dioxygenase pathway during bacterial infection of tobacco leaves. Formation of oxylipins protecting against cell death. J. Biol. Chem. 278:51796-51805.

Havelda, Z., Várallyay, E., Válóczi, A., and Burgyán, J. 2008. Plant virus infection-induced persistent host gene downregulation in systemically infected leaves. Plant J. 55(2):278-288.

Hernández, J. A., and Almansa, M. S. 2002. Short-term effects of salt stress on antioxidant systems and leaf water relations of pea plants. Physiol. Plant. 115:251-257.

Huang, Z., Yeakley, J. M., Garcia, E. W., Holdridge, J. D., Fan, J. B., and Whitham, S. A. 2005. Salicylic acid-dependent expression of host genes in compatible *Arabidopsis*–virus interactions. Plant Physiol. 137:1147-1159.

Hull, R. 2002. Matthews' Plant Virology. Academic Press, London.

Inskeep, W. P., and Bloom, P. R. 1985. Extinction coefficients of chlorophyll *a* and *b* in *N,N*-dimethylformamide and 80% acetone. Plant Physiol. 77(2):483-485.

Kasschau, K. D., Xie, Z., Allen, E., Llave, C., Chapman, E. J., Krizan, K. A., and Carrington, J. C. 2003. P1/HC-Pro, a viral suppressor of RNA silencing, interferes with *Arabidopsis* development and miRNA function. Dev. Cell. 4:205-217.

Kim, C. Y., and Zhang, S. 2004. Activation of a mitogen-activated protein kinase cascade induces WRKY family of transcription factors and defense genes in tobacco. Plant J. 38(1):142-151.

Kong, L. J., Orozco, M., Roe, J. L., Nagar, S., Ou, S., Feiler, H. S., Durfee, T., Miller, A. B., Gruissem, W., Robertson, D., and Hanley-Bowdoin, L. 2000. A geminvirus replication protein interacts with the retinoblastoma protein through a novel domain to determine symptoms and tissue specificity of infection in plants. EMBO (Eur. Mol. Biol. Organ.) J. 19:3485-3495.

Levine, R. L., Garland, D., Oliver, C. N., Amici, A., Climent, I., Lenz, A. G., Ahn, B., Shaltiel, S., and Stadtman, E. R. 1990. Determination of carbonyl content in oxidatively modified proteins. Methods Enzymol. 186:464-478.

Liu, Y., Schiff, M., and Dinesh-Kumar, S. P. 2002. Virus-induced gene silencing in tomato. Plant J. 31(6):777-786.

Liu, Y. D., Ren, D. T., Pike, S., Pallardy, S., Gassmann, W., and Zhang, S. Q. 2007. Chloroplast-generated reactive oxygen species are involved in hypersensitive response-like cell death mediated by a mitogen-activated protein kinase cascade. Plant J. 51:941-954.

Love, A. J., Yun, B. W., Laval, V., Loake, G. J., and Milner, J. J. 2005. *Cauliflower mosaic virus*, a compatible pathogen of *Arabidopsis*, engages three distinct defense-signaling pathways and activates rapid systemic generation of reactive oxygen species. Plant Physiol. 139:935-948.

Maere, S., Heymans, K., and Kuiper, M. 2005. BiNGO: A Cytoscape plugin to assess overrepresentation of Gene Ontology categories in biological networks. Bioinformatics 21(16):3448-3449.

Padmanabhan, M. S., Shiferaw, H., and Culver, J. N. 2006. The *Tobacco mosaic virus* replicase protein disrupts the localization and function of interacting Aux/IAA proteins. Mol. Plant-Microbe Interact. 19:864-873.

Pruss, G., Ge, X., Shi, X. M., Carrington, J. C., and Vance, V. B. 1997. Plant viral synergism: The potyviral genome encodes a broad-range pathogenicity enhancer that transactivates replication of heterologous viruses. Plant Cell 9:859-868.

Rensink, W. A., Iobst, S., Hart, A., Stegalkina, S., Liu, J., and Buell, C. R. 2005. Gene expression profiling of potato responses to cold, heat, and salt stress. Funct. Integr. Genomics. 5:201-207.

Riedle-Bauer, M. 2000. Role of reactive oxygen species and antioxidant enzymes in systemic virus infections of plants. J. Phytopathol. 148:297-302.

Rustérucci, C., Montillet, J. L., Agnel, J. P., Battesti, C., Alonso, B., Knoll, A., Bessoule, J. J., Etienne, P., Suty, L., Blein, J. P., and Triantaphylidés, C. 1999. Involvement of lipoxygenase-dependent production of fatty acid hydroperoxides in the development of the hypersensitive cell death induced by cryptogein on tobacco leaves. J. Biol. Chem. 274:36446-36455.

Schweighofer, A., and Meskiene, I. 2008. Regulation of stress hormones jasmonates and ethylene by MAPK pathways in plants. Mol. Biosyst. 4:799-803.

Senthil, G., Liu, H., Puram, V. G., Clark, A., Stromberg, A., and Goodin, M. M. 2005. Specific and common changes in *Nicotiana benthamiana* gene expression in response to infection by enveloped viruses. J. Gen. Virol. 86:2615-2625.

Smyth, G. K. 2004. Linear models and empirical bayes methods for assessing differential expression in microarray experiments. Stat. Appl. Genet. Mol. Biol. 3, Article 3. Published online.

Smyth, G. K., and Speed, T. 2003. Normalization of cDNA microarray data. Methods 31:265-273.

Técsi, L. I., Smith, A. M., Maule, A. J., and Leegood, R. C. 1996. A spatial analysis of physiological changes associated with infection of cotyle-

dons of marrow plants with *Cucumber mosaic virus*. Plant Physiol. 111:975-985.

Tenllado, F., and Díaz-Ruíz, J. R. 2001. Double-stranded RNA-mediated interference with plant virus infection. J. Virol. 75:12288-12297.

Thimm, O., Bläsing, O., Gibon, Y., Nagel, A., Meyer, S., Krüger, P., Selbig, J., Müller, L. A., Rhee, S. Y., and Stitt, M. 2004. MAPMAN: A user-driven tool to display genomics data sets onto diagrams of metabolic pathways and other biological processes. Plant J. 37:914-939.

Thompson, J. E., Froese, C. D., Madey, E., Smith, M. D., and Hong, Y. 1998. Lipid metabolism during plant senescence. Prog. Lipid Res. 37:119-141.

Turner, J.G., Ellis, C., and Devoto, A. 2002. The jasmonate signal pathway. Plant Cell 14 (Suppl.):S153-S164.

Vance, V. B. 1991. Replication of potato virus X RNA is altered in coinfections with potato virus Y. Virology 182:486-494.

Vanitharani, R., Chellappan, P., Pita, J. S., and Fauquet, C. M. 2004. Differential roles of AC2 and AC4 of cassava geminiviruses in mediating synergism and suppression of posttranscriptional gene silencing. J. Virol. 78:9487-9498.

Vellosillo, T., Martínez, M., López, M. A., Vicente, J., Cascón, T., Dolan, L., Hamberg, M., and Castresana, C. 2007. Oxylipins produced by the 9-lipoxygenase pathway in *Arabidopsis* regulate lateral root development and defense responses through a specific signaling cascade. Plant Cell 19:831-846.

Vollenweider, S., Weber, H., Stolz, S., Chételat, A., and Farmer, E. E. 2000. Fatty acid ketodienes and fatty acid ketotrienes: Michael addition acceptors that accumulate in wounded and diseased *Arabidopsis* leaves. Plant J. 24:467-476.

Wege, C., and Siegmund, D. 2007 Synergism of a DNA and an RNA virus: Enhanced tissue infiltration of the begomovirus *Abutilon mosaic virus* (AbMV) mediated by *Cucumber mosaic virus* (CMV). Virology 357:10-28.

Whitham, S. A., Quan, S., Chang, H. S., Cooper, B., Estes, B., Zhu, T., Wang, X., and Hou, Y. M. 2003. Diverse RNA viruses elicit the expression of common sets of genes in susceptible *Arabidopsis thaliana* plants. Plant J. 33:271-283.

Whitham, S. A., Yang, C., and Goodin, M. 2006. Global impact: Elucidating plant responses to viral infection. Mol. Plant-Microbe Interact. 19:1207-1215.

Yang C., Guo, R., Jie, F., Nettleton, D., Peng, J., Carr, T., Yeakley, J. M., Fan, J. B., and Whitham, S. A. 2007. Spatial analysis of *Arabidopsis thaliana* gene expression in response to *Turnip mosaic virus* infection. Mol. Plant-Microbe Interact. 20(4):358-370.

Yoshioka, H., Numata, N., Nakajima, K., Katou, S., Kawakita, K., Rowland, O., Jones, J. D., and Doke, N. 2003. *Nicotiana benthamiana* gp91^{phox} homologs *NbrbohA* and *NbrbohB* participate in H_2O_2 accumulation and resistance to *Phytophthora infestans*. Plant Cell 15:706-718.

Zhang, S., and Liu, Y. 2001. Activation of salicylic acid-induced protein kinase, a mitogen-activated protein kinase, induces multiple defense responses in tobacco. Plant Cell 13:1877-1889.

Zhang, S., Liu, Y., and Klessig, D. 2000. Multiple levels of tobacco WIPK activation during the induction of cell death by fungal elicitins. Plant J. 23:339-347.

Zhu, S., Gao, F., Cao, X., Chen, M., Ye, G., Wei, C., and Li, Y. 2005. The *Rice dwarf virus* P2 protein interacts with ent-kaurene oxidases in vivo, leading to reduced biosynthesis of gibberellins and rice dwarf symptoms. Plant Physiol. 139:1935-1945.

AUTHOR-RECOMMENDED INTERNET RESOURCES

The Institute for Genomic Research (TIGR) multi-experiment viewer software: www.tigr.org/software/tm4

The Biological Networks Gene Ontology (BiNGO) tool: www.psb.ugent.be/cbd/papers/BiNGO/index.htm

The MapMan visualization software: www.gabipd.org/projects/MapMan/